Sergio Elaskar
Professor
Instituto de Estudios Avanzados
en Ingeniería y Tecnología,
IDIT Departamento de Aeronáutica,
FCEFyN Universidad Nacional de Córdoba
and CONICET,
Córdoba 5000, Argentina
e-mail: selaskar@unc.edu.ar

Ezequiel del Río
Professor
E.T.S.I. Aeronáutica y Espacio,
Universidad Politécnica de Madrid,
Madrid 28040, Spain

Discontinuous Reinjection Probability Density Function in Type V Intermittency

This paper reports theoretical and numerical results about the reinjection process in type V intermittency. The M function methodology is applied to a simple mathematical model to evaluate the reinjection process through the reinjection probability density function (RPD), the probability density of laminar lengths, and the characteristic relation. We have found that the RPD can be a discontinuous function and it is a sum of exponential functions. The RPD shows two reinjection behaviors. Also, the probability density of laminar lengths has two different behaviors following the RPD function. The dependence of the RPD function and the probability density of laminar lengths with the reinjection mechanisms and the lower boundary of return are considered. On the other hand, we have obtained, for the analyzed map, that the characteristic relation verifies $\bar{l} \approx \varepsilon^{-0.5}$. *Finally, we highlight that the M function methodology is a suitable tool to analyze type V intermittency and there is a very high accuracy between the new theoretical equations and the numerical data.* [DOI: 10.1115/1.4041577]

1 Introduction

Chaos is an essential subject in engineering, biology, physics, chemistry, *etc*. Intermittency is a standard route to chaos, where trajectories alternate regular or laminar phases and chaotic bursts or nonregular phases. The laminar phases correspond to regions of pseudo-equilibrium or pseudo-periodic solutions, while the burst ones are regions where the trajectory is chaotic. Therefore, a system can evolve from regular to chaotic behavior by intermittency.

Traditionally, intermittency has been classified into three different types namely I, II, and III according to the system Floquet multipliers or to the local Poincaré map eigenvalues [1–4]. However, more recent research has included other intermittencies types such as V, X, on-off, in-out, eyelet, and ring [5–10].

Several physical phenomena show chaotic intermittency, like turbulent flows, Rayleigh-Bénard convection, forced nonlinear oscillators, plasma physics, and electronic circuits [11–19]. Additionally, intermittency was used to model the behavior in economics and medicine systems [20–22]. Therefore, a more accurate description of chaotic intermittency would help to improve the knowledge about all these phenomena.

Poincaré maps are useful tools to study chaotic intermittency [1,2,4]. The local map and the reinjection mechanism characterize the intermittency behavior. The local map is defined around the vanished or unstable fixed point. The reinjection mechanism maps back the trajectories from the chaotic zone to the laminar one, which is described by the reinjection probability density function (RPD). Then, the correct evaluation of the RPD function has considerable influence to describe the chaotic intermittency phenomenon accurately. The RPD function evaluation, from experimental or numerical data, is not a simple task due to the vast amount of data needed and the statistical fluctuations induced in the numerical computations and the experimental measurements. Accordingly, many approaches have been implemented to represent the RPD function, where the most common one was to consider a constant RPD (uniform reinjection). There were other approaches to build the RPD, but they used specific characteristics of the nonlinear processes, and these RPDs cannot successfully employ in other nonlinear systems [23,24].

The *M* function methodology, developed in the last years, is a broader methodology to evaluate RPD functions. It includes the uniform reinjection as a particular case, and it has shown to be very accurate for a broad class of maps showing type I, II, and III intermittencies [4,25–35]. This methodology has been recently applied to type V intermittency obtaining continuous and nonuniform RPDs [36]. In this paper, we implement the *M* function methodology to describe discontinuous RPD functions for type V intermittency. We show that this methodology works accurately for type V intermittency and the reinjection processes may include discontinuous RPDs. Besides, we find that the characteristic relations can acquire other forms than those previously published.

Baueret et al. [37,38] and Fan et al. [39] introduced type V intermittency, and it appears when a nondifferentiable point (NDP) and a stable fixed point collide forming a channel between the bisector line and the map. However, a tangent bifurcation does not happen because the local map is nondifferentiable or discontinuous at this point. We highlight that two maps with different slopes describing a "V" compose the local map.

The Hindmarsh–Rose model of neuronal activity showed type V intermittency [40–42]. The intermittent behavior displayed in the recurrence between irregular bursting and phases close to a period-3 bursting. The intermittent chaotic bursting and spiking from theoretical models and biological experiments were studied [41,42]. Therefore, the theoretical and numerical results introduced in this paper could help to improve the knowledge about these systems.

A review about type V intermittency has been recently carried out in Refs. [4] and [36].

2 Methods and Models

In this section, we first introduce a brief description of the *M* function methodology, which is a theoretical framework that describes the intermittency reinjection process for a broad class of maps and dynamical systems. Later, the piecewise one-dimensional map used in this paper is described.

2.1 The M Function Methodology. Evaluation of the Reinjection Probability Density Function. Let us consider a general one-dimensional map: $x_{n+1} = F(x_n)$. The RPD function, $\phi(x)$, specifies the probability density that trajectories are reinjected into a point x inside the laminar interval, i.e., the statistical behavior of the reinjection trajectories, which depends on the specific form of $F(x)$ [1,2,4].

Contributed by the Design Engineering Division of ASME for publication in the Journal of Computational and Nonlinear Dynamics. Manuscript received March 30, 2018; final manuscript received September 14, 2018; published online October 15, 2018. Assoc. Editor: Mohammad Younis.

In this methodology, the reinjection probability density function is not directly calculated from the data series. An auxiliary function, $M(x)$, is previously evaluated [4,25–30]

$$M(x) = \begin{cases} \dfrac{\int_{\hat{x}}^{x} \tau\phi(\tau)\,d\tau}{\int_{\hat{x}}^{x} \phi(\tau)\,d\tau}, & \text{if } \int_{\hat{x}}^{x} \phi(\tau)\,d\tau \neq 0, \\ 0, & \text{otherwise} \end{cases} \tag{1}$$

where $\hat{x}$ is the lower boundary of reinjection point, i.e., the closest reinjection point to the unstable fixed point.

The evaluation of $M(x)$ from numerical or experimental data series is straightforward:

$$M(x) \cong \frac{1}{N}\sum_{j=1}^{N} x_j \tag{2}$$

where the data set (reinjection points) $\{x_j\}_{j=1}^{N}$ must be sorted from the lowest to the highest, i.e., $x_j \leq x_{j+1}$ [25–32].

Previous studies have found that $M(x)$ satisfies a linear approximation for a broad class of maps showing type I, II, III, and V intermittencies [25–28,30,36]:

$$M(x) = \begin{cases} m(x-\hat{x}) + \hat{x}, & \text{if} \quad \hat{x} \leq x \leq c, \\ 0, & \text{otherwise}, \end{cases} \tag{3}$$

Note that the nonlinear map drives the reinjection process, and it determines the parameter $m \in (0, 1)$.

From Eqs. (1) and (3), the RPD function can be obtained [25,26,28,30,36]

$$\phi(x) = b(\alpha)(x-\hat{x})^{\alpha}, \quad \text{with} \quad \alpha = \frac{2m-1}{1-m} \tag{4}$$

where the normalization parameter, $b(\alpha)$, results

$$b(\alpha) = \frac{\alpha+1}{(c-\hat{x})^{\alpha+1}} \tag{5}$$

For $m = 1/2$ ($\alpha = 0$), the uniform RPD can be recovered, i.e., uniform reinjection is obtained as a particular case of the new theoretical formulation. However, the RPD can leave from the uniform reinjection, e.g., $\lim_{x\to 0}\phi(x)$ tends to zero, when $1/2 < m < 1$ ($\alpha > 0$) and to infinity when $0 < m < 1/2$ ($\alpha < 0$).

2.2 The Model: A Piecewise One-Dimensional Map. Maps defined on intervals of the real line are an essential tool in nonlinear dynamics and chaos [1,2,4,36,43]. In this work, we analyze piecewise maps, $F(x)$, described in the interval $y_0 \leq x \leq y_n$

$$F(x) = \begin{cases} f_1(x), & y_0 \leq x < y_1, \\ f_2(x), & y_1 \leq x < y_2, \\ \cdot & \\ \cdot & \\ \cdot & \\ f_n(x), & y_{n-1} \leq x \leq y_n \end{cases} \tag{6}$$

Let us consider a piecewise one-dimensional map showing type-V intermittency

$$F(x) = \begin{cases} F_1(x) = a_1 x + \varepsilon, & \tilde{x} \leq x < 0, \\ F_2(x) = \varepsilon + x + a_2 x^2, & 0 \leq x < x_m, \\ F_3(x) = \tilde{x} + \dfrac{(y_m - \tilde{x})(y_m - x)^{\gamma}}{(y_m - x_m)^{\gamma}}, & x_m \leq x \leq y_m \end{cases} \tag{7}$$

where $y_m = F(x_m) = 1$, $\tilde{x}$ is the lower boundary of return [4,36], $0 < a_1 < 1$ is the slope of the straight line, a_2 is the coefficient of the quadratic term in $F_2(x)$, and finally ε is the control parameter. If $\tilde{x} = 0$, the map is defined inside the interval [0, 1]. Note that $F_1(x)$ is a linear function and $F_2(x)$ corresponds to the local map for type I intermittency. The $F_3(x)$ function generates the reinjection process, and it depends on the exponent γ. Therefore, this map allows analyzing distinct types of reinjection mechanisms using different values of γ. Figure 1 shows the map.

This map was used in Ref. [36] to describe nonuniform RPDs for type V intermittency. Here, we obtain discontinuous RPDs only modifying the lower boundary of return.

The map can have three fixed points

$$\begin{aligned} x_1 &= \frac{\varepsilon}{1-a_1}, \\ x_2 &= \left(\frac{-\varepsilon}{a_2}\right)^{0.5}, \\ x_3 &= \tilde{x} + \frac{(1-\tilde{x})(1-x_3)^{\gamma}}{(1-x_m)^{\gamma}} \end{aligned} \tag{8}$$

If $\varepsilon < 0$, the fixed point x_1 is less than zero and x_2 is higher than zero. Also, x_1 and x_2 disappear for $\varepsilon > 0$, and they are equal zero if $\varepsilon = 0$. For $\varepsilon = 0$, the fixed points x_1 and x_2 collide in one fixed point $x_0 = 0$.

The map (7) has a nondifferentiable point at $x = 0$, which collides with the fixed point x_0 for $\varepsilon = 0$. The fixed point vanishes and type-V intermittency can appear for $0 < \varepsilon \ll 1$.

The iteration procedure–governed by a_1, a_2 and ε–gives increasing values of x_n generated from an initial one, close to $F(\tilde{x})$. A chaotic burst–govern by $F_2(x)$ and $F_3(x)$—occurs when $x > 0$ becomes large enough, ending when the trajectory is reinjected into a point inside the laminar zone. Then, a new iterative process–governed by ε, a_1 and a_2 is developed producing larger values of the new successive iterative points.

In a previous paper, we considered reinjection processes where the lower boundary of return is equal to the lower boundary of the laminar interval [36]. Therefore, we could study type V intermittency with continuous and nonuniform RPDs. Now, we shall analyze tests in which the lower boundary of return does not match the lower boundary of the laminar interval, more

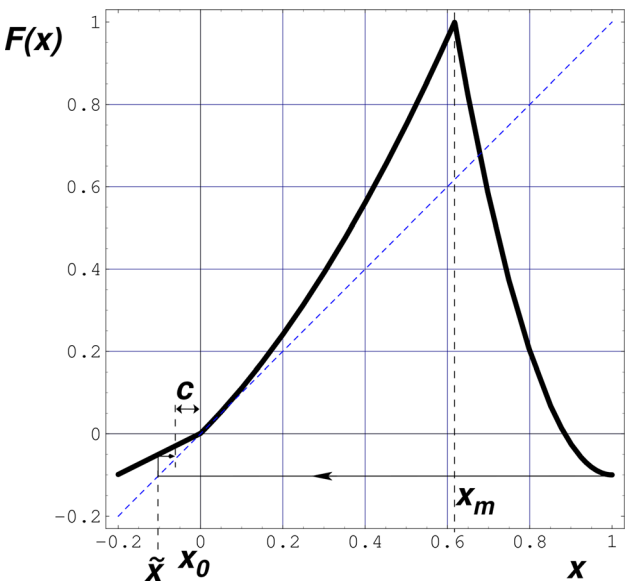

Fig. 1 Map described by Eq. (7). The parameters are $\gamma = 2$, $\varepsilon = 0.001$, $a_1 = 0.5$, $a_2 = 1$. x_0 is the vanished fixed point and $\tilde{x}$ is the lower boundary of return. A trajectory moving through $\tilde{x}$ is also indicated.

specifically $\tilde{x} < x_0 - c$ (where $x_0 - c$ is the lower boundary of the laminar interval). Then, trajectories coming from $\tilde{x} \leq x < x_0 - c$ could reinject in the laminar interval. Therefore, two different cases can appear:

(a) All trajectories passing through the lower boundary of return match the lower boundary of the laminar interval: $F^n(\tilde{x}) = x_0 - c$ for some n.
(b) No iteration of the lower boundary of return matches the lower boundary of the laminar interval: $F^n(\tilde{x}) \neq x_0 - c$ for all n.

To study the intermittency behavior in this map, we shall carry out several numerical experiments or tests considering different reinjection processes for the case (a). Note that we can always turn a case (b) into a case (a) by moving the laminar interval slightly.

3 Results

We consider three tests, which verify $F^n(\tilde{x}) = x_0 - c$ for some n. The first test uses the following parameters: $\gamma = 1$, $\varepsilon = 0.001$, $a_1 = 0.9$, $a_2 = 1$, $N_j = 30{,}000$, $c = 0.1128$ and $\tilde{x} = -1.00006$. N_j is the number of reinjected points. Note that $\tilde{x} = F^{-20}(x_0 - c)$. Therefore, for this test, there are two reinjection mechanisms. One of them is directly generated by $F_3(x)$ in Eq. (7); this mechanism is the same one evaluated in Ref. [36]. The second mechanism corresponds to points reinjected from values $x < x_0 - c$. Then, some points placed in the interval $[\tilde{x}, x_0 - c)$ will be reinjected in the interval $\Delta_1 = [x_0 - c, x_s)$, being $x_s = F(x_0 - c)$ a singular point where $M(x)$ is a nondifferentiable function. Note that Δ_1 is a subinterval of the laminar interval $[x_0 - c, x_0 + c]$ [4,31].

Figure 2 shows the bifurcation diagram for the map (7) with $\gamma = 1$, $a_1 = 0.9$, $a_2 = 1$ and $\tilde{x} = -1.00006$. The clearer points indicate the chaotic behavior for the first test (see Figs. 3–7). From the figure, there is a stable fixed point for $\varepsilon < 0$; however, for $\varepsilon > 0$, there is chaotic behavior. To describe this behavior, we show in Fig. 8(*b*) the evolution of the map iterations (time series) corresponding to the clearer points in Fig. 2 ($\varepsilon = 0.001 > 0$). From this figure, we can observe intermittency. Figure 8(*a*) shows the time evolution for $\varepsilon = -0.001 < 0$; for this case, the fixed point $x_0 = x_1$ is stable.

Figure 3 shows the numerical and theoretical $M(x)$ functions. The theoretical $M(x)$ function is calculated using Eq. (1). In this figure, the laminar interval is divided into two subintervals: $\Delta_1 = [x_0 - c,\ x_s)$ and $\Delta_2 = [x_s,\ x_0 + c]$. Δ_1 possesses reinjected points coming from $x < x_0 - c$ and from $x > x_m > x_0 + c$. However, the interval Δ_2 only receives points from $x > x_m > x_0 + c$.

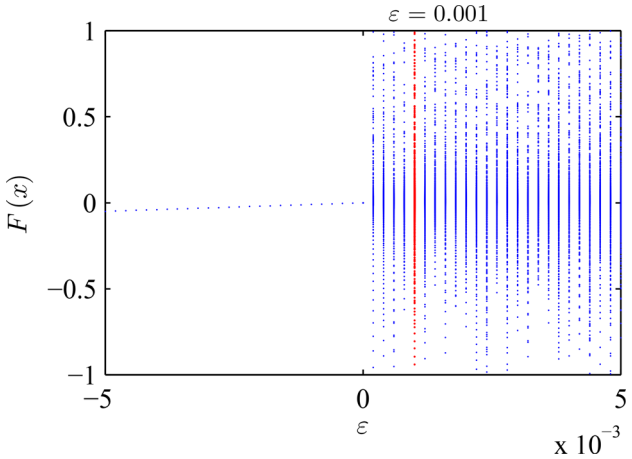

Fig. 2 Bifurcation diagram for map (7) with $\gamma = 1$, $a_1 = 0.9$, $a_2 = 1$ and $\tilde{x} = -1.00006$. Clearer points correspond with the first numerical test.

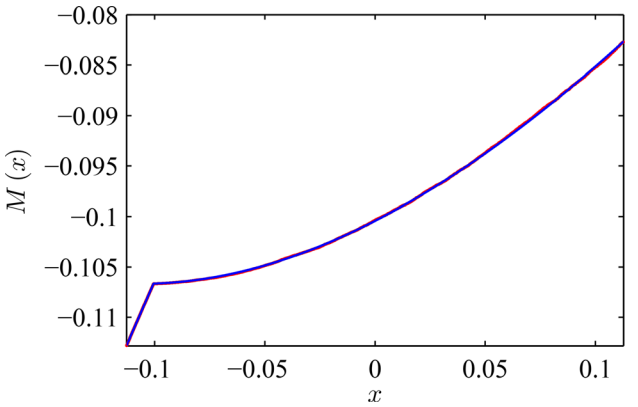

Fig. 3 $M(x)$ function for map (7) with $\gamma = 1$, $\varepsilon = 0.001$, $a_1 = 0.9$, $a_2 = 1$, $N_j = 30{,}000$, $c = 0.1128$ and $\tilde{x} = -1.00006$. Clearer line is the numerical data and the continuous line represents the theoretical $M(x)$ function.

Figures 4 and 5 show the $M(x)$ functions inside the intervals $\Delta_1 = [x_0 - c, x_s)$ and $\Delta = [x_0 - c, x_0 + c]$ respectively. Note that to obtain Fig. 5, reinjected points coming from $x > x_m$ are only considered. Points reinjected from $x < x_0 - c$ are placed inside

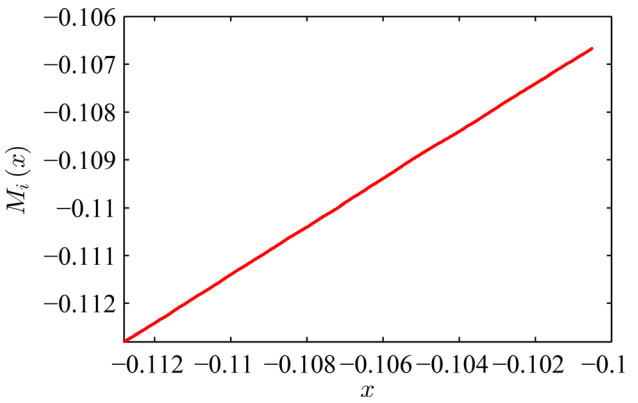

Fig. 4 Numerical $M_i(x)$ function $\Delta_1 = [x_0 - c,\ x_s]$ for map (7) calculated using only reinjected points coming from $x < x_0 - c$. Parameters: $\gamma = 1$, $\varepsilon = 0.001$, $a_1 = 0.9$, $a_2 = 1$, $N_j = 30{,}000$, $c = 0.1128$ and $\tilde{x} = -1.00006$. From this figure we obtain: $m_i \cong 0.5006$ and $\alpha_i \cong -0.00249$.

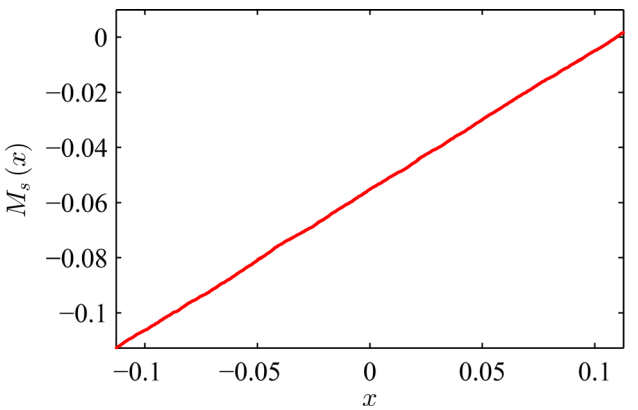

Fig. 5 Numerical $M_s(x)$ function inside $\Delta = [x_0 - c,\ x_0 + c]$ for map (7) obtained for reinjected points coming from $x > x_m$. Parameters: $\gamma = 1$, $\varepsilon = 0.001$, $a_1 = 0.9$, $a_2 = 1$, $N_j = 30{,}000$, $c = 0.1128$ and $\tilde{x} = -1.00006$. From this figure we calculate: $m_s \cong 0.5089$ and $\alpha_s \cong 0.03623$.

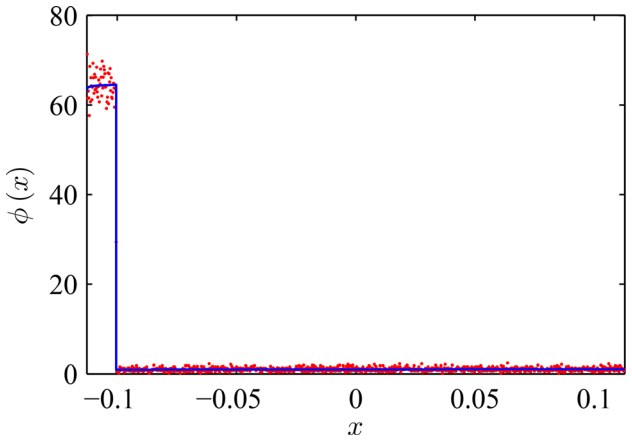

Fig. 6 RPD for map (7) with $\gamma = 1$, $\varepsilon = 0.001$, $a_1 = 0.9$, $a_2 = 1$, $N_j = 30{,}000$, $c = 0.1128$ and $\tilde{x} = -1.00006$. Points are numerical results and the continuous line represents the theoretical RPD calculated using Eqs. (9)–(11).

the subinterval Δ_1; the numerical function $M_i(x)$ is calculated only using these points. $M_i(x)$ is a linear function with slope $m_i \cong 0.5006$ and $\alpha_i \cong -0.00249$ (see Fig. 4). Points reinjected from $x > x_m > x_0 + c$ are distributed along all the laminar intervals $[x_0 - c,\ x_0 + c]$; the numerical $M_s(x)$ function is evaluated using these points, and it is shown in Fig. 5, which is also a linear function ($m_s \cong 0.5089$ and $\alpha_s \cong 0.03623$).

As the $M(x)$ function has a nondifferentiable point (see Fig. 3), the RPD is discontinuous at this point. With $\phi_1(x)$, we restrict the analysis to the interval $[x_0 - c,\ x_s)$ and with $\phi_2(x)$, we consider only points $x \geq x_s$ (see Eq. (9)). Therefore, the RPD results:

$$\phi(x) = \begin{cases} \phi_1(x) = \phi_i(x) + \phi_s(x), & x_0 - c \leq x < x_s, \\ \phi_2(x) = \phi_s(x), & x_s \leq x \leq x_0 + c \end{cases} \tag{9}$$

where

$$\begin{aligned} \phi_i(x) &= b\,(x - x_0 + c)^{\alpha_i}, \\ \phi_s(x) &= b\,k\,(x - x_0 + c)^{\alpha_s} \end{aligned} \tag{10}$$

The RPD, $\phi(x)$, is obtained by superimposing two reinjection processes represented by $\phi_i(x)$ and $\phi_s(x)$, where $\phi_i(x)$ and $\phi_s(x)$ are calculated using trajectories coming from $x < x_0 - c$ and $x > x_0 + c$, respectively.

To find the parameters m_i and m_s, we first sort the numerical data and apply the M function methodology as described in Sec. 2. Then, we can calculate the functions $\phi_i(x)$ and $\phi_s(x)$ using Eq. (10).

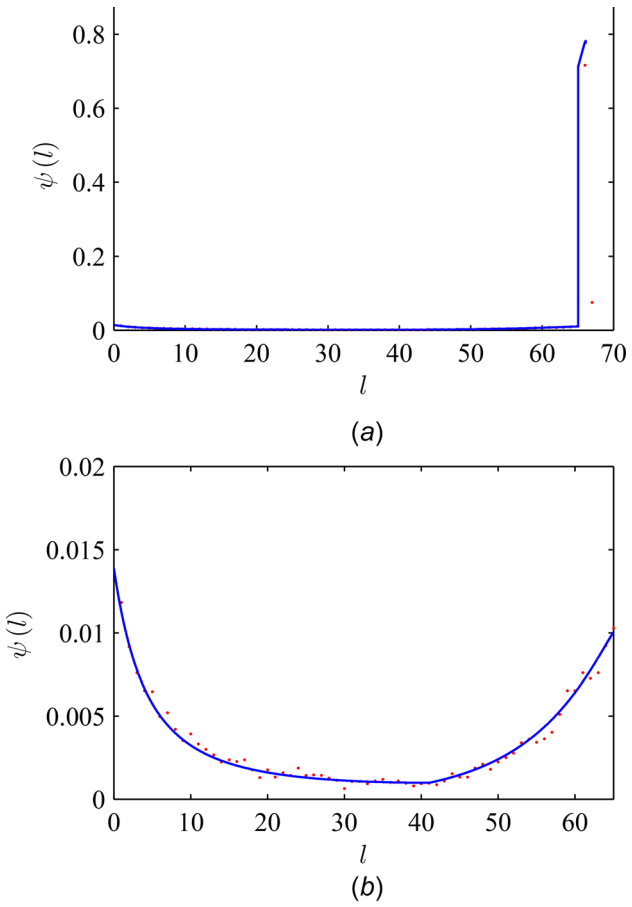

Fig. 7 Probability density of the laminar length for $\gamma = 1$, $\varepsilon = 0.001$, $a_1 = 0.9$, $a_2 = 1$, $N_j = 30{,}000$, $c = 0.1128$ and $\tilde{x} = -1.00006$. Points represent the numerical data, and the line the theoretical results calculated using Eqs. (9), (10), (18) and (19). (*b*) is an enlargement of (*a*) for reinjected points inside of Δ_2 interval.

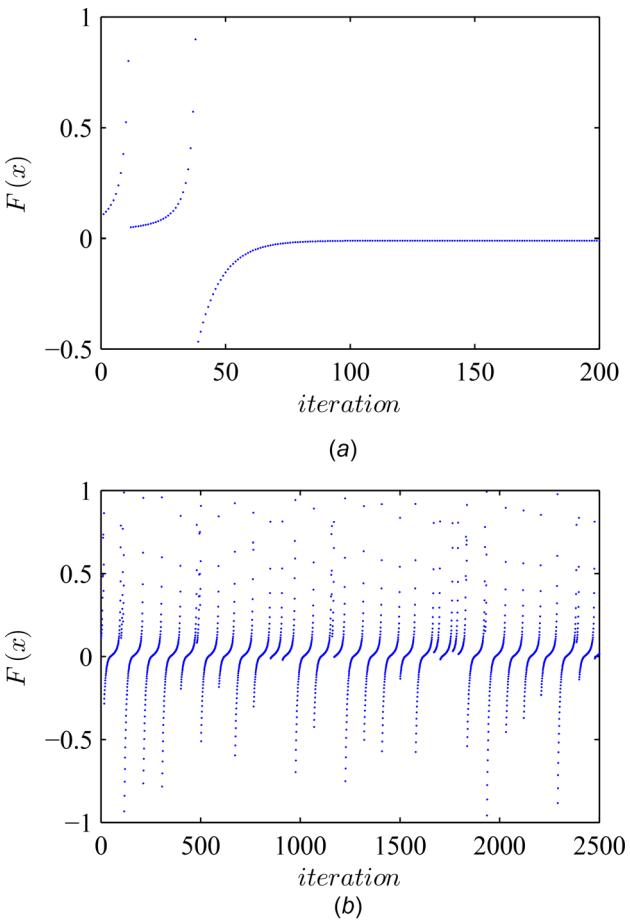

Fig. 8 Iterative evolution of the map (7) with $\gamma = 1$, $a_1 = 0.9$, $a_2 = 1$ and $\tilde{x} = -1.00006$. (*a*) uses $\varepsilon = -0.001 < 0$ and $x_0 = x_1$ is a stable fixed point. (*b*) considers $\varepsilon = 0.001 > 0$, the iterative process shows intermittency.

Consequently, the exponents α_i and α_s are obtained from

$$\alpha_{i,s} = \frac{2m_{i,s} - 1}{1 - m_{i,s}} \tag{11}$$

being m_i the slope of the following function:

$$M_i(x) = m_i(x - x_0 + c) + x_0 - c \tag{12}$$

which is defined in $[x_0 - c, x_s)$, and it considers only reinjected points coming from $x < x_0 - c$; and m_s is the slope of

$$M_s(x) = m_s(x - x_0 + c) + x_0 - c \tag{13}$$

which is calculated using only reinjected points coming from $x > x_m > x_0 + c$ and it is defined in $[x_0 - c, x_0 + c]$.

The factor b is the normalization parameter, and it results

$$b = \left(\frac{(x_s - x_0 + c)^{1+\alpha_i}}{1 + \alpha_i} + k \frac{(2c)^{1+\alpha_s}}{1 + \alpha_s} \right)^{-1} \tag{14}$$

To obtain the global $M(x)$ function, we again apply the M function methodology described in Sec. 2. Then, Eqs. (15) and (16) give the global $M(x)$ function. We highlight that this function has a nondifferentiable point at $x = x_s$.

The factor k, in Eq. (10), is used to evaluate the different number of reinjections in the interval Δ_1 with respect those for Δ_2. This parameter is obtained using the definition of $M(x)$. Because the global $M(x)$ function does not depend on the parameter b, we can obtain the factor k from it. To carry out this task, the global $M(x)$ function should be evaluated at some point $x_y > x_s$, i.e., $M_y = M(x_y)$. Then, it is possible to explicitly obtain the factor k, which is expressed by Eq. (17). In a few cases, it could be necessary to calculate k using the Eq. (17) evaluated at two points called (x_{y1}, M_{y1}) and (x_{y2}, M_{y2}); the factor k will be the mean value: $k = 0.5(k_1 + k_2)$.

For $x_0 - c \le x < x_s$

$$M(x) = \frac{\int_{x_0-c}^{x} \tau\, \phi_i(\tau)\, d\tau + \int_{x_0-c}^{x} \tau\, \phi_s(\tau)\, d\tau}{\int_{x_0-c}^{x} \phi_i(\tau)\, d\tau + \int_{x_0-c}^{x} \phi_s(\tau)\, d\tau} = \frac{\dfrac{(c+x)^{1+\alpha_i}(-c + x(1+\alpha_i))}{(1+\alpha_i)(2+\alpha_i)} + \dfrac{k(c+x)^{1+\alpha_s}(-c + x(1+\alpha_s))}{(1+\alpha_s)(2+\alpha_s)}}{(c+x)^{1+\alpha_i}(1+\alpha_i)^{-1} + k(c+x)^{1+\alpha_s}(1+\alpha_s)^{-1}} \tag{15}$$

For $x \ge x_s$

$$\begin{aligned} M(x) &= \frac{\int_{x_0-c}^{x_s} \tau\, \phi_i(\tau)\, d\tau + \int_{x_0-c}^{x_s} \tau\, \phi_s(\tau)\, d\tau + \int_{x_s}^{x} \tau\, \phi_s(\tau)\, d\tau}{\int_{x_0-c}^{x_s} \phi_i(\tau)\, d\tau + \int_{x_0-c}^{x_s} \phi_s(\tau)\, d\tau + \int_{x_s}^{x} \phi_s(\tau)\, d\tau} \\ &= \frac{(c+x_s)^{1+\alpha_i}(-c + x_s(1+\alpha_i))[(1+\alpha_i)(2+\alpha_i)]^{-1} + [x_s + (1+\alpha) - c][(1+\alpha_s)(2+\alpha_s)]^{-1}\left[(k-1)(c+x_s)^{1+\alpha_s} + k(c+x)^{1+\alpha_s}\right]}{(c+x_s)^{1+\alpha_i}(1+\alpha_i)^{-1} + k(c+x)^{1+\alpha_s}(1+\alpha_s)^{-1}} \end{aligned} \tag{16}$$

$$k = \frac{1+\alpha_s}{1+\alpha_i} \frac{\left((x_s - x_0 + c)^{1+\alpha_i}\right)(x_s(1+\alpha_i) + x_0 - c)(2+\alpha_i)^{-1} - M_y(x_s - x_0 + c)^{1+\alpha_i})}{M_y(x_y - x_0 + c)^{1+\alpha_s} - \left((x_y - x_0 + c)^{1+\alpha_s}\right)\left(x_y(1+\alpha_s) + x_0 - c\right)(2+\alpha_s)^{-1}} \tag{17}$$

Figures 3 and 6 show the global nondifferentiable $M(x)$ and the discontinuous RPD functions respectively for $\gamma = 1$, $\varepsilon = 0.001$, $a_1 = 0.9$, $a_2 = 1$, $N_j = 30{,}000$, $c = 0.1128$ and $\tilde{x} = -1.00006$. From these figures, we can observe a very good accuracy between the numerical data and the theoretical Eqs. (9), (10), (11), (15) and (16).

Another useful statistical function to describe chaotic intermittency is the probability density of the laminar lengths, $\psi(l)$, which is a global property of the map [1,4]. The laminar length, $l(x, c)$, is the number of iterations that a trajectory performs inside the laminar interval; and the probability density of the laminar lengths gives the probability of finding laminar lengths between l and $l + dl$ [1,4]

$$\psi(l, c) = \phi[X(l, c)] \left| \frac{dX(l, c)}{dl} \right| \tag{18}$$

where $X(l, c)$ is the inverse of $l(x, c)$. For the map (7), $(dX(l, c)/dl)$ can be approximated by (if $\varepsilon \ll 1$ and $a_1 < 1$ but close to 1)

$$\begin{aligned} \frac{dX(l, c)}{dl} &= \varepsilon + x(a_1 - 1), \quad x < 0, \\ \frac{dX(l, c)}{dl} &= \varepsilon + a_2 x^2, \quad x \ge 0 \end{aligned} \tag{19}$$

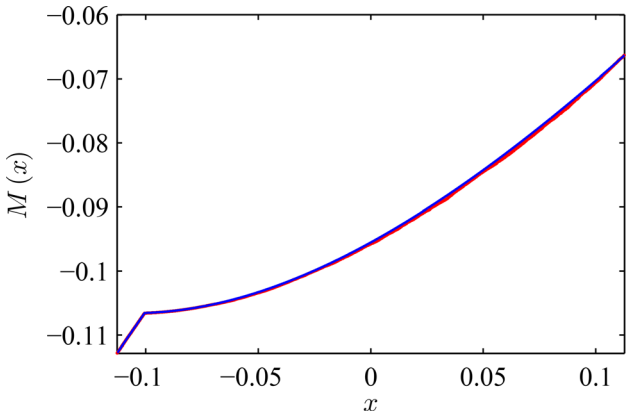

Fig. 9 Function $M(x)$ for map (7). The parameters are: $\gamma = 0.5$, $\varepsilon = 0.001$, $a_1 = 0.9$, $a_2 = 1$, $N_j = 30{,}000$, $c = 0.1128$ and $\tilde{x} = -1.00006$. Clearer line is obtained from numerical data, and the darker one is calculated using Eqs. (15)–(17).

Note that $dX(l, c)/dl$ is a nondifferentiable function. From Eqs. (19), $l(x, c)$ can be evaluated

$$l(x,c) = \left[\ln(\varepsilon) - \ln((a_1-1)x+\varepsilon)\right] \times (a_1-1)^{-1} + (a_2\varepsilon)^{-1/2} \arctan\left(c\frac{\sqrt{a_2}}{\sqrt{\varepsilon}}\right), \quad x < 0,$$

$$l(x,c) = \left[\arctan\left(c\frac{\sqrt{a_2}}{\sqrt{\varepsilon}}\right) - \arctan\left(x\frac{\sqrt{a_2}}{\sqrt{\varepsilon}}\right)\right](a_2\varepsilon)^{-1/2}, \quad x \geq 0 \tag{20}$$

Figures 7(*a*) and 7(*b*) show $\psi(l)$ for the same parameters of the previous figures. Points represent the numerical data, and the line is the theoretical result calculated using Eqs. (9), (10), (18) and (19). Figure 7(*b*) is an enlargement of Fig. 7(*a*), which only shows $\psi(l)$ for points reinjected inside of Δ_2 interval. The probability density of the laminar lengths has two behaviors, one for $l \leq 65$ corresponding to the reinjections in the interval Δ_2, and other one for $l > 65$ for reinjections in the interval Δ_1. We can observe a very good accuracy between numerical data and theoretical results.

This test shows that a discontinuous RPD function can appear in type V intermittency. The laminar interval has two subintervals with different RPD inside each one. It is a new behavior, different from those previously described [36–39]. However, the RPD is constant in each subinterval.

To evaluate a nonconstant RPD in each interval, we consider a reinjection process governed by $\gamma \neq 1$. We use the same parameters of the previous test, but now $\gamma = 0.5$. Figures 9 and 10 show the numerical and theoretical $M(x)$ and RPD functions. Line corresponds to theoretical results and the numerical data are indicated in red. Again, the laminar interval has two subintervals, $\Delta_1 = [x_0 - c, x_s)$ and $\Delta_2 = [x_s, x_0 + c]$, where $M(x)$ and $\phi(x)$ have different behaviors. Therefore, to evaluate the theoretical RPD, we have implemented the M function methodology described by Eqs. (9)–(17). Figure 10(*b*) is an enlarged image of Fig. 10(*a*) inside the Δ_2 interval.

To obtain the exponents α_i and $\alpha_{s,}$ we use the numerical data show in Figs. 11 and 12 respectively: $\alpha_i \cong 0.0389$ $(m_i \cong 0.5095)$ and $\alpha_s \cong 0.08847$ $(m_s \cong 0.5212)$.

From Figs. 10(*a*) and 10(*b*), we can note that the RPD inside each subinterval $\Delta_1 = [x_0 - c, x_s)$ and $\Delta_2 = [x_s, x_0 + c]$ increases as x increases. Also, the theoretical results have a high accuracy with respect the numerical data.

Figure 13 shows the probability density of the laminar lengths, calculated by Eq. (18), for the same parameters as the previous figures. Note the outstanding accuracy between the numerical data with the analytical results.

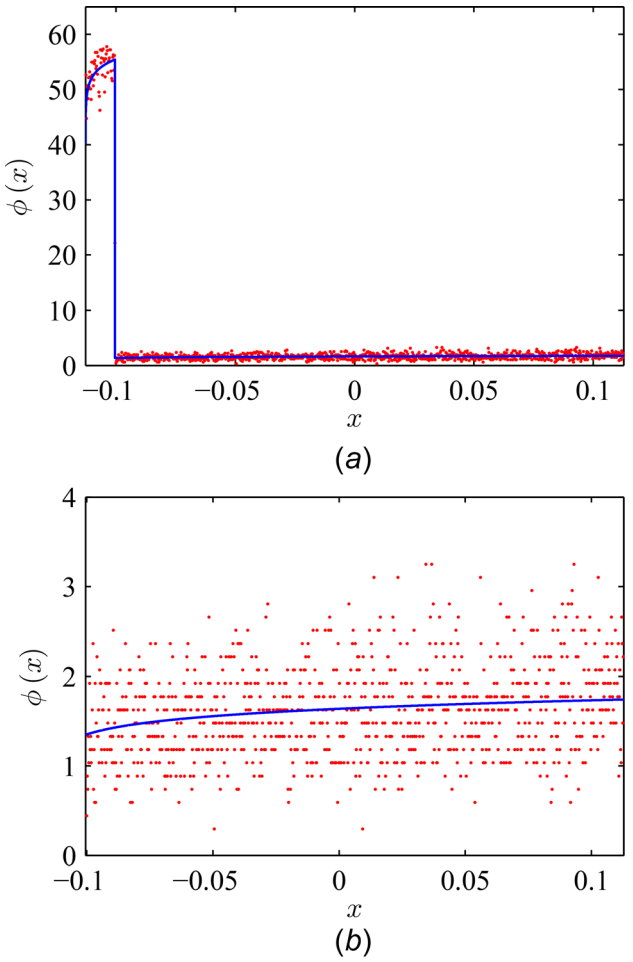

Fig. 10 RPD for map (7). The parameters are: $\gamma = 0.5$, $\varepsilon = 0.001$, $a_1 = 0.9$, $a_2 = 1$, $N_j = 30{,}000$, $c = 0.1128$ and $\tilde{x} = -1.00006$. Points represent the numerical data, and the continuous line corresponds to the theoretical RPD calculated using Eqs. (9)–(11). (*b*) is an enlarged image of the (*a*) inside the Δ_2 interval.

Furthermore, we carried out several numerical tests with $\gamma = 1.5$ using the M function methodology to obtain the RPD function. Similarly to the previous cases, the RPDs are discontinuous.

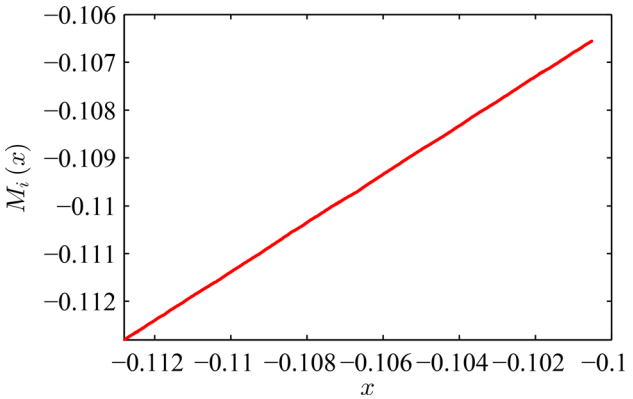

Fig. 11 Numerical $M_i(x)$ function inside $\Delta_1 = [x_0 - c, x_s)$ for map (7) obtained using only reinjected points coming from $x < x_0 - c$. The parameters are: $\gamma = 0.5$, $\varepsilon = 0.001$, $a_1 = 0.9$, $a_2 = 1$, $N_j = 30{,}000$, $c = 0.1128$ and $\tilde{x} = -1.00006$. $M_i(x)$ is a linear function with slope $m_i \cong 0.5095$.

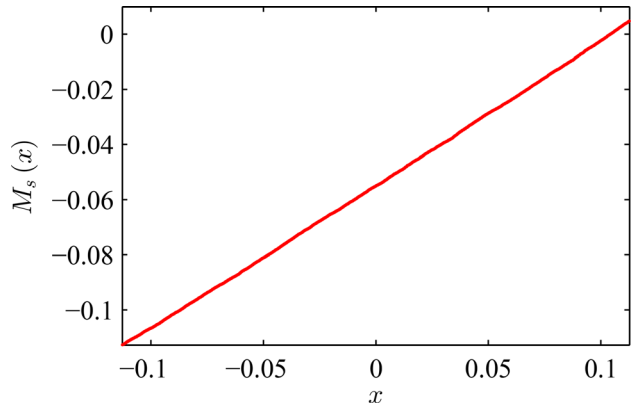

Fig. 12 Numerical $M_s(x)$ function inside $\Delta_2 = [x_s,\ x_0 + c]$ for map (7) obtained for reinjected points coming from $x > x_m$. The parameters are: $\gamma = 0.5$, $\varepsilon = 0.001$, $a_1 = 0.9$, $a_2 = 1$, $N_j = 30{,}000$, $c = 0.1128$ and $\tilde{x} = -1.00006$. $M_s(x)$ is a linear function with slope $m_s \cong 0.5212$.

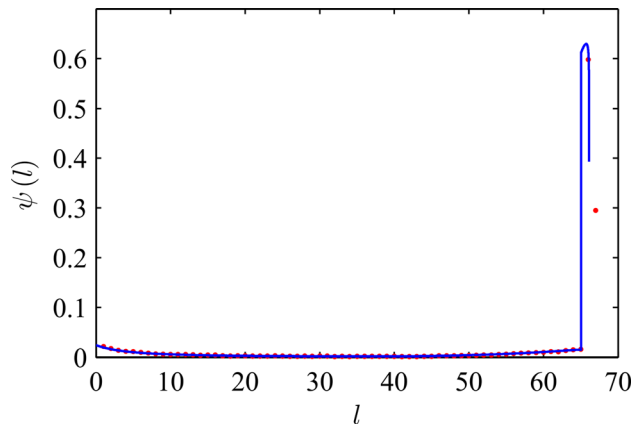

Fig. 13 Probability density of the laminar length, $\psi(l)$, for map (7). The parameters are: $\gamma = 0.5$, $\varepsilon = 0.001$, $a_1 = 0.9$, $a_2 = 1$, $N_j = 30{,}000$, $c = 0.1128$ and $\tilde{x} = -1.00006$. Points represent the numerical data, and the line the theoretical results calculated using Eqs. (9), (10), (18) and (19).

Tables 1 and 2 show the values of α_i and α_s for $\gamma = 0.5$, 1, 1.5 and for two lower boundaries of return $\tilde{x} = -1.00006$ and $\tilde{x} = -0.15844993141289437$.

From these tables, we can note that α_i and α_s depend on γ. For $\gamma < 1$, α_i and α_s are higher than 0; for $\gamma = 1$, $\alpha_i \cong \alpha_s \cong 0$; and for $\gamma > 1$, α_i and α_s are lower than 0. Also, we can observe that α_i and α_s depend on $\tilde{x}$. Therefore, the reinjection process, i.e., α_i and α_s, depends on $dF_3(x)/dx$ valuated at different points: a—around $x = y_m$, b—for $F^{-1}(x_0 - c) \le x \le F^{-1}(x_0 + c)$, i.e., around $x = F^{-1}(x_0)$ (see Refs. [4] and [34]).

3.1 Influence of the Lower Boundary of Return. This section analyzes the influence of the lower boundary of return, $\tilde{x}$, on the reinjection process. To carry out this task, the lower boundary of return can get different values, but the other parameters do not change.

Table 1 α_i, α_s, m_i and m_s for different values of γ. The other parameters are $\varepsilon = 0.001$, $a_1 = 0.9$, $a_2 = 1$, $N_j = 30{,}000$, $c = 0.1128$ and $\tilde{x} = -1.00006$.

γ	α_i	α_s	m_i	m_s
0.5	0.0389	0.08847	0.5095	0.5212
1.0	0.00249	0.03623	0.5006	0.508897
1.5	−0.082642	−0.03137	0.47845	0.492032

Table 2 α_i, α_s, m_i and m_s for different values of γ. The other parameters are $\varepsilon = 0.001$, $a_1 = 0.9$, $a_2 = 1$, $N_j = 30{,}000$, $c = 0.1128$ and $\tilde{x} = -0.15844993141289437$.

γ	α_i	α_s	m_i	m_s
0.5	0.30308	0.70238	0.5658	0.62995
1.0	−0.00651	0.00597	0.49837	0.50148
1.5	−0.2037	−0.14965	0.4433	0.45956

Table 3 α_i and α_s for different values of $\tilde{x}$. The parameters are $\gamma = 1.5$, $\varepsilon = 0.001$, $a_1 = 0.9$, $a_2 = 1$, $N_j = 30{,}000$, and $c = 0.1128$. The last column indicates the number of needed iterations from $\tilde{x}$ to $x_0 - c$.

$\tilde{x}$	α_i	α_s	Iterations
−0.126444444444444	−0.33774	−0.20727	1
−0.158449931412894	−0.20367	−0.14965	3
−0.342186145207406	−0.1084	−0.05874	10
−0.6527	−0.0856	−0.00871	16
−1.00006	−0.08264	−0.03137	20

The first test set uses the following parameters: $\gamma = 1.5$, $\varepsilon = 0.001$, $a_1 = 0.9$, $a_2 = 1$, $N_j = 30{,}000$, $c = 0.1128$ and different $\tilde{x}$. The results are summarized in Table 3

If we consider that the lower boundary of return matches the lower limit of the laminar interval, $\tilde{x} = x_0 - c$, there in not reinjection from $x < x_0 - c$; and the only reinjection process is produced by $x > x_m$. In this case, the following relation should be satisfied [4,25,34]:

$$\alpha = \frac{1}{\gamma} - 1 \tag{21}$$

On the other hand, also α_s is influenced by $\tilde{x}$, because α_s depends on the reinjection trajectories coming from $F_3(x)$. When $\tilde{x} \to -\infty$, the function $F_3(x_n)$ is almost linear with constant and finite $|dF_3(x_n)/dx|$, where $x_{n+1} = F(x_n)$ are the reinjected points. Therefore, when $\tilde{x} \to -\infty$, $\alpha_s \to 0$. Conversely, when $\tilde{x}$ approaches to $x_0 - c$, then $\alpha_s \neq 0$.

Hence, it is important to highlight that the distance between the lower boundary of return, $\tilde{x}$, and the lower limit of the laminar interval, $x_0 - c$, has a strong influence on the reinjection process.

3.2 The Characteristic Relation. The characteristic relation sets the relationship between the average laminar length, $\bar{l}$, and the control parameter, ε. The average laminar length is [4]

$$\bar{l} = \int_{x_0 - c}^{x_0 + c} \phi(x) l(x, c) dx \tag{22}$$

where $\phi(x)$ and $l(x, c)$ are given by Eqs. (9) and (20), respectively. For $x_s \le x_0$, the average laminar length results

$$\bar{l} = \bar{l}_1 + \bar{l}_2 + \bar{l}_3 \tag{23}$$

where

$$\begin{aligned} \bar{l}_1 &= \int_{x_0 - c}^{x_s} \phi_1(x)\, l(x, c)|_{x < x_0} dx \\ \bar{l}_2 &= \int_{x_s}^{x_0} \phi_2(x)\, l(x, c)|_{x < x_0} dx \\ \bar{l}_3 &= \int_{x_0}^{x_0 + c} \phi_2(x)\, l(x, c)|_{x > x_0} dx \end{aligned} \tag{24}$$

The last equation only possesses analytical solution in few cases, such as: $\alpha_i = \alpha_s = 0$ and $\alpha_i = \alpha_s = 1$. For $\alpha_i = \alpha_s = 0$, the relations between $\bar{l}_1$, $\bar{l}_2$, $\bar{l}_3$, and ε are settled down in Eqs. (25), (26), and (27) respectively.

$$\bar{l}_1 = b(1+k)\left[\left((a_1-1)^{-1}\ln(\varepsilon) + \arctan\left(c\sqrt{\frac{a_2}{\varepsilon}}\right)(a_2\,\varepsilon)^{-1/2}\right)\times(c+x_s) + (c+x_s)(a_1-1)^{-1}\right] - (a_1-1)^{-2}b(1+k)[(\varepsilon+(a_1-1)x_s)\ln(\varepsilon+(a_1-1)x_s) - (\varepsilon-(a_1-1)c)\ln(\varepsilon-(a_1-1)c)] \tag{25}$$

$$\bar{l}_2 = -b\,k\left[x_s + \frac{\ln(\varepsilon)}{a_1-1}\left(\frac{\varepsilon}{a_1-1}+x_s\right) - \frac{(\varepsilon+(a_1-1)x_s)\ln(\varepsilon+(a_1-1)x_s)}{(a_1-1)^2} + \frac{\arctan\left(c\sqrt{\frac{a_2}{\varepsilon}}\right)}{a_2\varepsilon}\right] \tag{26}$$

$$\bar{l}_3 = \frac{0.5\,b\,k\left[\ln(\varepsilon + a_2\,c^2) - \ln(\varepsilon)\right]}{a_2} \tag{27}$$

Figure 14 shows the relation $\ln(\bar{l}) = \bar{l}(\ln(\varepsilon))$, i.e., the characteristic relation. The line represents the theoretical results given by Eqs. (23)–(27), and the red points are the numerical data. Note the outstanding accuracy between the numerical and theoretical results. A linear function with slope $s_n \approx s_t \approx -0.47$ can express the characteristic relation (where s_n corresponds to the numerical data and s_t to the theoretical approach). Therefore, the characteristic relation results

$$\bar{l} = \varepsilon^{-\beta} \tag{28}$$

with $\beta \approx 0.5$. We highlight although the RPD is discontinuous, the characteristic relation still satisfies Eq. (28).

We can find another analytical expression for the characteristic relation if we assume $\alpha_i = \alpha_s = 1$. This last condition could be verified when $F_1(\tilde{x}) = x_0 - c$ and $\gamma = 0.5$, but in this case, the number of reinjected points from $x < x_0 - c$ is very much reduced (less than 1 for 300 global reinjections) and the accurate evaluation of parameters k and b is very difficult. Note that the theoretical characteristic relation has a strong dependence on b and k; then the results are susceptible with the number of reinjected points from $x < x_0 - c$. As the relation between reinjected points from $x < x_0 - c$ and the total reinjected points is minimal, we can introduce errors in the analytical evaluation. Therefore, we calculate the characteristic relations using direct numerical integration. Besides the numerical integration of both, theoretical and numerical results, allows us to use different values of γ (not only $\gamma = 0$ or $\gamma = 1$).

We study several tests with $\gamma = 1.5$ and $\varepsilon = 0.001 - 0.0000001$. To obtain $\bar{l}$, we use Eqs. (9), (18) and (19), from which we carry out the numerical calculation of the following integral:

$$\bar{l} = \int_0^{l_m} \psi(l)\, l\, dl \tag{29}$$

We consider two sets of tests. Both groups have similar parameters, and they only differ in the number of iterations that the trajectories need to reinject from $\tilde{x}$ to $x_0 - c$. For the first test, the reinjection process from $\tilde{x}$ to $x < x - 0 - c$ needs 20 iterations. The second one uses $F_1(\tilde{x}) = x_0 - c$; therefore, the process needs only one iteration to reinject from points $x < x_0 - c$. Table 4 shows $\tilde{x}$ for different ε.

Figure 15 shows the results. The upper and lower lines correspond for tests with 20 and 1 iterations between $\tilde{x}$ and $x_0 - c$. In both cases, points and lines represent the numerical and theoretical results, respectively, which have a very high accuracy. When trajectories need only 1 iteration to be reinjected (lower line), the numerical and theoretical slopes are $s_n \cong -0.46$ and $s_t \cong -0.467$. On the other hand, for trajectories with 20 iterations, the slopes are: $s_n \cong s_t \cong -0.47$. Also, for these cases, Eq. (28) is verified with $\beta \approx 0.5$.

Table 4 $\tilde{x}$, α_i and α_s for different values of $\tilde{x}$ to maintain 1 iteration from $\tilde{x}$ to $x = x_0 - c$. The parameters are $\gamma = 1.5$, $a_1 = 0.9$, $a_2 = 1$, $N_j = 30{,}000$, and $c = 0.1128$.

ε	$\tilde{x}$	α_i	α_s
0.001	−0.126444	−0.3306678	−0.201
0.0001	−0.125444	−0.3306678	−0.201
0.00001	−0.125344	−0.34637	−0.2241
0.000001	−0.125334	−0.3292	−0.2112
0.0000001	−0.125333	−0.324895	−0.21541

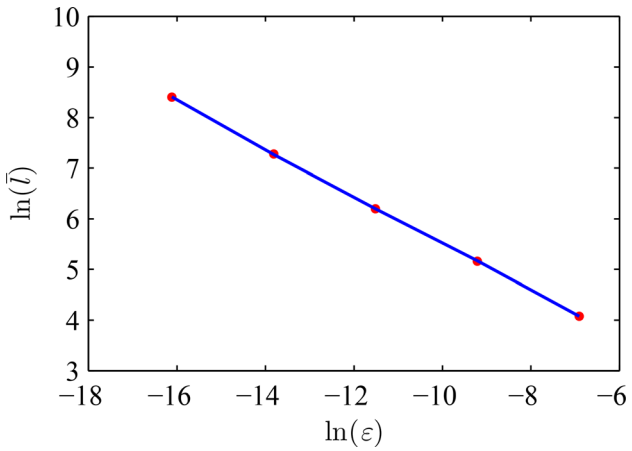

Fig. 14 Characteristic relation for $\gamma = 1$, $\varepsilon = 0.001$–0.0000001, $a_1 = 0.9$, $a_2 = 1$, the number of iterations from $\tilde{x}$ to $x_0 - c$ is 20. Points: numerical data. Line: theoretical approach given by Eqs. (23)–(27).

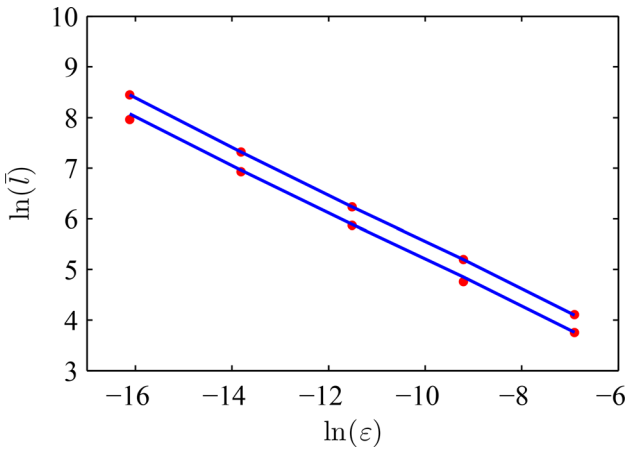

Fig. 15 Characteristic relation for $\gamma = 1.5$, $\varepsilon = 0.001$–0.0000001, $a_1 = 0.9$, $a_2 = 1$. The number of iterations from $\tilde{x}$ to $x_0 - c$ are 1 and 20 for the lower and upper lines respectively. Points: numerical data. Line: theoretical approach.

Table 5 $\tilde{x}$, α_i and α_s for different values of $\tilde{x}$ to maintain 20 iterations from $\tilde{x}$ to $x = x_0 - c$. The parameters are $\gamma = 1.5$, $a_1 = 0.9$, $a_2 = 1$, $N_j = 30{,}000$, and $c = 0.1128$.

ε	$\tilde{x}$	α_i	α_s
0.001	−1.00006	−0.082642	−0.031372
0.0001	−0.935031	−0.10182	−0.0215356
0.00001	−0.92853	−0.0879117	−0.012836
0.000001	−0.92788	−0.065915	−0.0201744
0.0000001	−0.927816	−0.08006	−0.0236215

The average laminar length is higher for trajectories needing 20 iterations to go from the $\tilde{x}$ to the laminar interval in comparison with those needing only 1 iteration (see Fig. 15). It happens because the reinjection processes, govern by α_i and α_s, are different. Tables 4 and 5 give α_i and α_s. When the process needs only one iteration $\alpha_i \approx -0.33$ and $\alpha_s \approx -0.21$; however, when it needs 20 iterations, $\alpha_i \approx \alpha_s \approx 0$. Therefore, $\bar{l}$ acquires similar values for processes with $\gamma = 1.5$ and trajectories with 20 iterations from $\tilde{x}$ to $x_0 - c$ and processes with $\gamma = 1$. The $\tilde{x}$ influence on the RPD and other functions, such as the characteristic relation, is significant because as the distance $|\tilde{x} - (x_0 - c)|$ increases the influence of γ reduces.

We emphasize that three tests with different values of γ and $\tilde{x}$ were analyzed, and the characteristic relation $\bar{l} \approx \varepsilon^{-0.5}$ was verified.

4 Analysis and Conclusions

We applied the M function methodology to describe the reinjection process for type V intermittency. This methodology had worked accurately for type I, II, and III intermittencies where the local map is continuous, and for type V intermittency with continuous RPD. In this paper, we have shown that this methodology also works accurately for type V intermittency with discontinuous RPDs. It can capture very well the RPD function, and other intermittency statistical properties (probability density of the laminar lengths and average laminar length), for different reinjection mechanisms.

Two elementary functions compose the local map of Eq. (7), one is linear and the other one quadratic. The used laminar interval was symmetrical around the vanished fixed point. We have shown that, even for this simple map, the RPD can be a discontinuous function. It happens because there are two reinjection mechanisms if the lower boundary of return is less than the lower limit of the laminar interval, $\tilde{x} < x_0 - c$. One of them is produced by trajectories coming from points $x < x_0 - c$, and the other one from trajectories coming from $x > x_m > x_0 + c$.

The laminar interval has two subintervals, within each one of them the RPD function has different behavior. The subintervals are $\Delta_1 = [x_0 - c,\ x_s)$ and $\Delta_2 = [x_s,\ x_0 + c]$, being x_s is a singular point where the RPD is discontinuous. Δ_1 receives trajectories coming from $x < x_0 - c$ and $x > x_m$; however, Δ_2 only receives trajectories from $x > x_m$. The RPD is a sum of exponential functions with exponents α_i and α_s, to obtain its analytical expression is only necessary to evaluate the slope m_i and m_s of the $M(x)$ function where m_i and m_s are calculated using reinjected points from $x < x_0 - c$ and $x > x_m$ respectively.

We have evaluated the influence of the lower boundary of return, $\tilde{x}$, on the RPD. We have found that $\tilde{x}$ has a substantial impact on the RPD: when the distance $|\tilde{x} - (x_0 - c)|$ increases the influence of γ reduces, and the reinjection process resembles the reinjection process for $\gamma = 1$.

Besides, the influence of γ on the RPD was studied. The exponents α_i and α_s decrease when γ increases, and $\alpha_i \approx \alpha_s \approx 0$ for $\gamma = 1$. However, in all cases, the RPD is discontinuous.

Similarly to the RPD, the probability density of the laminar lengths also has two distinctive behaviors, one for reinjections inside the subinterval Δ_1 and the other one for reinjections in the subinterval Δ_2.

For all analyzed tests, with different values of γ and $\tilde{x}$, the characteristic relation could be written as: $\bar{l} \approx \varepsilon^{-0.5}$.

Finally, we highlight that the obtained theoretical equations for the reinjection probability density, the probability density of the laminar lengths, and the characteristic relation showed an outstanding accuracy regarding the numerical data for different values of γ, ε, and $\tilde{x}$.

Acknowledgment

This research was supported by CONICET, Universidad Nacional de Córdoba, Universidad Politécnica de Madrid, and the Spanish Ministry of Science and Innovation (MICINN) under Project No. EPS2013-41078-R.

References

[1] Schuster, H., and Just, W., 2005, *Deterministic Chaos*, Wiley VCH, Mörlenbach, Germany.
[2] Nayfeh, A., and Balachandran, B., 1995, *Applied Nonlinear Dynamics*, Wiley, New York.
[3] Marek, M., and Schreiber, I., 1995, *Chaotic Behaviour of Deterministic Dissipative Systems*, Cambridge University Press, Cambridge, UK.
[4] Elaskar, S., and del Rio, E., 2017, *New Advances on Chaotic Intermittency and Its Applications*, Springer, New York.
[5] Kaplan, H., 1992, "Return to Type-I Intermittency," Phys. Rev. Lett., **68**(5), pp. 553–557.
[6] Price, T., and Mullin, P., 1991, "An Experimental Observation of a New Type of Intermittency," Phys. D, **48**(1), pp. 29–52.
[7] Platt, N., Spiegel, E., and Tresser, C., 1993, "On-Off Intermittency: A Mechanism for Bursting," Phys. Rev. Lett., **70**(3), pp. 279–282.
[8] Pikovsky, A., Osipov, G., Rosenblum, M., and Zaks, M. J. K., 1997, "Attractor-Repeller Collision and Eyelet Intermittency at the Transition to Phase Synchronization," Phys. Rev. Lett., **79**(1), pp. 47–50.
[9] Lee, K., Kwak, Y., and Lim, T., 1998, "Phase Jumps Near a Phase Synchronization Transition in Systems of Two Coupled Chaotic Oscillators," Phys. Rev. Lett., **81**(2), pp. 321–324.
[10] Hramov, A., Koronovskii, A., Kurovskaya, M., and Boccaletti, S., 2006, "Ring Intermittency in Coupled Chaotic Oscillators at the Boundary of Phase Synchronization," Phys. Rev. Lett., **97**, p. 114101.
[11] Dubois, M., Rubio, M., and Berge, P., 1983, "Experimental Evidence of Intermittencies Associated With a Subharmonic Bifurcation," Phys. Rev. Lett., **51**, p. 1446.
[12] Malasoma, J., Werny, P., and Boiron, M., 2004, "Multichannel Type-I Intermittency in Two Models of Rayleigh-Benard Convection," Phys. Rev. Lett., **51**(3), pp. 487–500.
[13] Stavrinides, S., Miliou, A., Laopoulos, T., A., and Anagnostopoulos, A., 2008, "The Intermittency Route to Chaos of an Electronic Digital Oscillator," Int. J. Bifurcation Chaos, **18**(5), pp. 1561–1566.
[14] Sanmartin, J., Lopez-Rebollal, O., del Rio, E., and Elaskar, S., 2004, "Hard Transition to Chaotic Dynamics in Alfven Wave-Fronts," Phys. Plasmas, **11**(5), pp. 2026–2035.
[15] Sanchez-Arriaga, G., Sanmartin, J., and Elaskar, S., 2007, "Damping Models in the Truncated Derivative Nonlinear Schrödinger Equation," Phys. Plasmas, **14**(8), p. 082108.
[16] Pizza, G., Frouzakis, G., and Mantzaras, J., 2012, "Chaotic Dynamics in Premixed Hydrogen/Air Channel Flow Combustion," Combust. Theor. Model, **16**(2), pp. 275–299.
[17] Nishiura, Y., Ueyama, D., and Yanagita, T., 2005, "Chaotic Pulses for Discrete Reaction Diffusion Systems," SIAM J. Appl. Dyn. Syst., **4**(3), pp. 723–754.
[18] de Anna, P., Borgne, T. L., Dentz, M., Tartakovsky, A., Bolster, D., and Davy, P., 2013, "Flow Intermittency, Dispersion and Correlated Continuous Time Random Walks in Porous Media," Phys. Rev. Lett., **110**, p. 184502.
[19] Stan, C., Cristescu, C., and Dimitriu, D., 2010, "Analysis of the Intermittency Behavior in a Low-Temperature Discharge Plasma by Recurrence Plot Quantification," Phys. Plasmas, **17**(4), p. 042115.
[20] Chian, A., 2007, *Complex System Approach to Economic Dynamics* (Lecture Notes in Economics and Mathematical Systems, Vol. 592), Springer, Berlin.
[21] Zebrowski, J., and Baranowski, R., 2004, "Type-I Intermittency in Nonstationary Systems: Models and Human Heart-Rate Variability," Phys. A, **336**(1-2), pp. 74–86.
[22] Paradisi, P., Allegrini, P., Gemignani, A., Laurino, M., Menicucci, D., and Piarulli, A., 2012, "Scaling and Intermittency of Brains Events as a Manifestation of Consciousness," AIP Conference Proceedings, **1510**(1), p. 151.
[23] Kye, W., and Kim, C., 2000, "Characteristic Relations of Type-I Intermittency in Presence of Noise," Phys. Rev. E, **62** (5 Pt A), pp. 6304–6307.
[24] Kye, W., Rim, S., Kim, C., Lee, J., Ryu, J., Yeom, B., and Park, Y., 2003, "Experimental Observation of Characteristic Relations of Type-III

Intermittency in the Presence of Noise in a Simple Electronic Circuit," Phys. Rev. E, **68**(3) p. 036203.
[25] del Rio, E., and Elaskar, S., 2010, "New Characteristic Relation in Type-II Intermittency," Int. J. Bifurcation Chaos, **20**(4), pp. 1185–1191.
[26] Elaskar, S., del Rio, E., and Donoso, J., 2011, "Reinjection Probability Density in Type-III Intermittency," Phys. A, **390**(15), pp. 2759–2768.
[27] del Rio, E., Sanjuan, M., and Elaskar, S., 2012, "Effect of Noise on the Reinjection Probability Density in Intermittency," Commun. Nonlinear Sci. Numer. Simul., **17**(9), pp. 3587–3596.
[28] Elaskar, S., and del Rio, E., 2012, "Intermittency Reinjection Probability Function With and Without Noise Effects," Latest Trends in Circuits, Automatics Control and Signal Processing, WSEAS, Barcelona, Spain, pp. 145–154.
[29] del Rio, E., Elaskar, S., and Makarov, V., 2013, "Theory of Intermittency Applied to Classical Pathological Cases," Chaos, **23**(3), p. 033112.
[30] del Rio, E., Elaskar, S., and Donoso, J., 2014, "Laminar Length and Characteristic Relation in Type-I Intermittency," Commun. Nonlinear Sci. Numer. Simul., **19**(4), pp. 967–976.
[31] Krause, G., Elaskar, S., and del Rio, E., 2014, "Type-I Intermittency With Discontinuous Reinjection Probability Density in a Truncation Model of the Derivative Nonlinear Schrödinger Equation," Nonlinear Dyn., **77**(3), pp. 455–466.
[32] Krause, G., Elaskar, S., and del Rio, E., 2014, "Noise Effect on Statistical Properties of Type-I Intermittency," Phys. A, **402**, pp. 318–329.
[33] Elaskar, S., del Rio, E., Krause, G., and Costa, A., 2015, "Effect of the Lower Boundary of Reinjection and Noise in Type-II Intermittency," Nonlinear Dyn., **79**(2), pp. 1411–1424.
[34] del Rio, E., and Elaskar, S., 2016, "On the Intermittency Theory in 1D Maps," Int. J. Bifurcation Chaos, **26**(14), p. 1620228.
[35] Elaskar, S., del Rio, E., and Costa, A., 2017, "Reinjection Probability Density for Type-III Intermittency With Noise and Lower Boundary of Reinjection," ASME J. Comput. Nonlinear Dyn., **12**(3), p. 031020.
[36] Elaskar, S., del Rio, E., and Marcantoni, L. G., 2018, "Nonuniform Reinjection Probability Density Function in Type V Intermittency," Nonlinear Dyn., **92**, pp. 683–697.
[37] Bauer, M., Habip, S., He, D., and Martiessen, W., 1992, "New Type of Intermittency in Discontinuous Maps," Phys. Rev. Lett., **68**(11), pp. 1625–1628.
[38] He, D., Bauer, M., Habip, S., Kruger, U., Martiessen, W., Christiansen, B., and Wang, B., 1992, "New Type of Intermittency in Discontinuous Maps," Phys. Lett. A, **171**(1–2), pp. 61–65.
[39] Fan, J., Ji, F., Guan, S., Wang, B., and He, D., 1993, "Type V Intermittency," Phys. Lett. A, **182**(2–3), pp. 232–237.
[40] Wu, S., and He, D., 2001, "Characteristics of Period-Doubling Bifurcation Cascades in Quasidiscontinuous Systems," Commun. Theor. Phys., **35**(3), pp. 275–282.
[41] Wang, D., Mo, J., Zhao, X., Gu, H., Qu, S., and Ren, W., 2011, "Intermittent Chaotic Neural Firing Characterized by Non-Smooth like Features," Chin. Phys. Lett., **27**(7), p. 070503.
[42] Gu, H., and Xiao, W., 2014, "Difference Between Intermittent Chaotic Bursting and Spiking of Neural Firing Patterns," Int. J. Bifurcation Chaos, **24**(6), p. 1450082.
[43] Bai-lin, H., 1989, *Elementary Symbolic Dynamics Chaos Dissipative Systems*, World Scientific, Singapore.